Raymo, M.E., Jansen, E., Blum, P., and Herbert, T.D. (Eds.), 1999
Proceedings of the Ocean Drilling Program, Scientific Results, Vol. 162

14. LOW-FREQUENCY OSCILLATIONS IN SITE 983 SEDIMENTS: RELATIONSHIPS BETWEEN CARBONATE AND PRODUCTIVITY PROXIES[1]

Sangmin Hyun,[2, 3] Joseph D. Ortiz,[4] M.E. Raymo,[5] and Asahiko Taira[2]

ABSTRACT

A geochemical study of sediments from Ocean Drilling Program Site 983 was conducted to examine low-frequency variations in carbonate content as expressed by blue-band reflectance (450–500 nm) over the last 1.2 Ma. Sedimentary percent organic carbon, percent carbonate, and excess barium (Ba[ex]) were used as the primary tools to evaluate the factors responsible for these long-term changes. We observe positive correlation between the mass-accumulation rate of various biogenic components and the mass-accumulation rate of Ba(ex), especially in sediments younger than ~600 ka. Deeper in the section (~600–1200 ka), the correlation between Ba(ex) and the other biogenic tracers is weak. The lack of correlation between Ba(ex) and biogenic carbonate likely results either from a higher supply of terrigenous material at that time (which confounds Ba[ex] estimation), or remobilization of Ba resulting from low pore-water sulfate ion concentrations, or both. Nonbiogenic sediments at Site 983, represented by Th, K_2O, and the molar Ti/Al ratio, exhibit cyclic variations that represent mixing between continental and oceanic (i.e., basaltic) terrigenous sources. The timing of these cycles matches that of the major glacial–interglacial cycles, which suggests that they result from the supply of continental material as ice-rafted debris during glacial periods and fine-grained basaltic material by bottom currents during interglacial periods. Given these observations, the most likely causes for the low-frequency carbonate variations observed in the Site 983 sediments are shifts in surface productivity and, to a lesser extent, dilution by the input of terrigenous material.

INTRODUCTION

Color-reflectance measurement of split-core surfaces on board ship during Ocean Drilling Program Leg 162 provided a rapid, sensitive means of characterizing lithologic variability. At Site 983, shipboard spectral reflectance data demonstrated low-frequency oscillations that were driven by variations in carbonate content (Ortiz et al., Chap. 19, this volume). Possible causes for these low-frequency carbonate oscillations include (1) time-dependent changes in oceanic productivity, (2) carbonate dissolution, or (3) carbonate dilution by terrigenous material. We performed a low-resolution paleoproductivity study of the last 1.2 m.y. at Site 983 to determine whether the observed low-frequency carbonate variations were related to changes in productivity. Total organic carbon, percent carbonate, excess barium (denoted as Ba[ex]), and a suite of major and minor geochemical elements were used to accomplish this task.

GEOLOGIC SETTING

Site 983 was drilled on the Gardar Drift (Fig. 1), a sediment drift deposited on the eastern flank of the Reykjanes Ridge along the northwest margin of the Iceland Basin. The northward flow of warm, saline North Atlantic surface water between Iceland and the Shetland Islands (Norwegian Current) and the southward flow of cold, polar surface water and ice through the Fram Strait (East Greenland Current) are the most prominent surface currents affecting this location. Sediments recovered from Site 983 are characterized by cyclic deposition of marine biogenic particles, ice-rafted debris (IRD), and redeposited fine-grained material carried by bottom currents associated with Iceland-Scotland Overflow Water (ISOW). There is no evidence of significant sediment disturbance or erosion at this site, although moderate bioturbation is present throughout.

The high sedimentation rate at this drift site provides an unprecedented record of both glacial–interglacial and millennial-scale variations in thermohaline circulation, surface-water temperature, and ice-rafting history during the late Pliocene and Pleistocene (e.g., Raymo et al., 1998). These high-frequency oscillations are superimposed on the long-term variability that is the focus of this study.

METHODS AND MATERIALS

All the shore-based analytical work presented here was conducted at the Ocean Research Institute, University of Tokyo. Shipboard spectral reflectance observations sparked the initial idea for this post-cruise geochemical study. Spectral reflectance data for Site 983 were generated during Leg 162 using an updated version of the split-core analysis track (SCAT), an automated reflectance spectrometer developed at Oregon State University and first described by Mix et al. (1992). A description of the revised instrument can be found in Ortiz et al. (Chap. 19, this volume). The instrument measures light reflected off the wet surface of a split core in the wavelength range from 250 to 950 nm using a 1024-channel detector. Calibration of the instrument to yield absolute reflectance is achieved using both internal and external standards.

Sediment color can be used to delineate the extent of oxic and anoxic sediment conditions as well as lithologic composition because sediment brightness usually depends on carbonate content (Nagano and Nakashima, 1992; Mix et al., 1992; Harris et al., 1997; Ortiz et al., Chap. 19, this volume). Although carbonate such as that produced by marine foraminifers and coccolithophorids is highly reflective across all visible wavelengths of light, it tends to exhibit reflectance maxima in the blue wavelength range from 450 to 500 nm (Mix et al., 1992). Blue-band reflectance is thus well correlated with percent carbonate (Fig. 2A). For that reason, we used the 450–500 nm blue-band reflectance data generated by the SCAT to guide our choice of sam-

[1]Raymo, M.E., Jansen, E., Blum, P., and Herbert, T.D. (Eds.), 1999. *Proc. ODP, Sci. Results*, 162: College Station, TX (Ocean Drilling Program).
[2]Ocean Research Institute, University of Tokyo, 1-15-1 Minamidai, Nakano-ku, Tokyo 164, Japan.
[3]Present address: Korea Ocean Research and Development Institute (KORDI), Ansan, P.O. Box 29, Seoul 425-600, Korea. smhyun@sari.kordi.re.kr
[4]Lamont-Doherty Earth Observatory of Columbia University, Route 9W, Palisades, NY 10964, U.S.A.
[5]Department of Earth, Atmospheric, and Planetary Sciences, Massachusetts Institute of Technology E34-254, Cambridge, MA 02139, U.S.A.

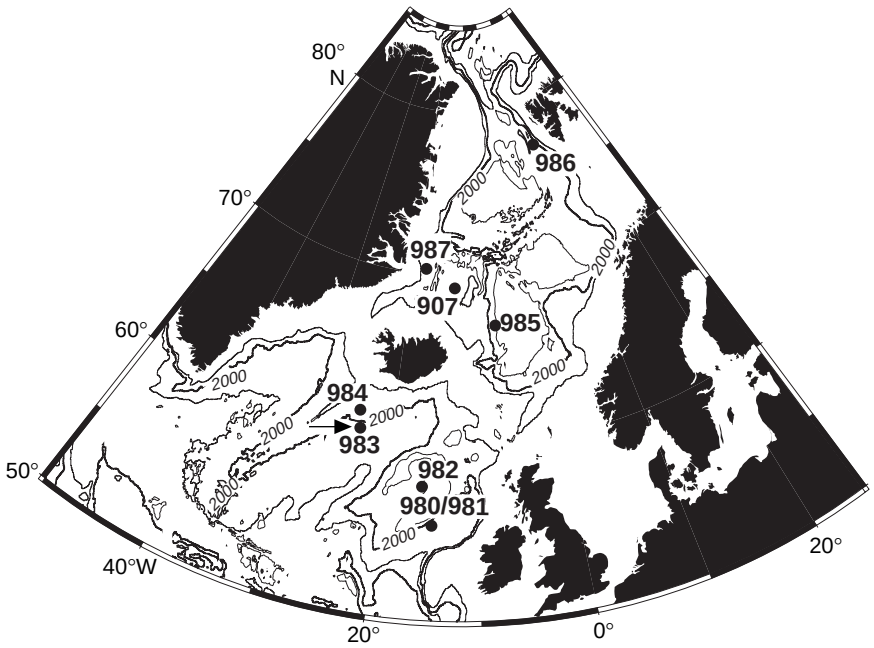

Figure 1. Map of the North Atlantic showing Leg 162 sites (arrow indicates Site 983). Bathymetric contours for 1000, 2000, and 3000 m water depth are indicated (after Jansen, Raymo, Blum, et al., 1996).

pling intervals. A total of 65 discrete samples were selected from peaks and troughs in the spliced reflectance record from Site 983 for in-depth geochemical analysis (Fig. 2B). Because each sample was taken from a sediment interval with a matching reflectance measurement, the discrete samples provided carbonate data to calibrate the spliced SCAT measurements at this site. This allowed us to obtain a high-resolution proxy carbonate record by simple linear regression:

$$\text{proxy\% carbonate} = 3.13 \times (\text{blue reflectance\%}) - 11.74.$$

The regression has an r^2 value of 0.84 and a root mean square error of 4.07%. This calibration is valid for percent blue reflectance values >3.75%. Below that threshold, sediment lightness is independent of carbonate content. The reflectance-based proxy percent carbonate data thus allowed us to determine high-resolution $CaCO_3$ mass-accumulation rates.

To determine the age of sediments from 0 to 90 meters composite depth (mcd), we used an age model based on oxygen isotope data from Channell et al. (1998) and J. McManus (unpubl. data). This age model consists of 30 isotope events derived from a 1444-sample planktonic foraminiferal oxygen isotope record. This yields an average temporal resolution of ~25 k.y. between age control points. For comparison, the age resolution of our discrete samples is ~18 k.y. Below 90 mcd, we relied on shipboard magnetostratigraphic and biostratigraphic datums (Jansen, Raymo, Blum, et al., 1996). Used in conjunction with the shipboard physical properties bulk density measurements (Jansen, Raymo, Blum, et al., 1996), this age model allowed us to generate mass-accumulation rates for study of the low-frequency variability observed in these sediments. This age model and its associated mass-accumulation rates are sufficient for this low-resolution study. The age-control points, sedimentation rates, and the ages of each discrete sample are provided in Tables 1 and 2.

Bulk Sediment Composition

Splits of the sediment samples were dried and powdered for total carbon (TC) and total organic carbon (TOC) analysis (Table 3). Defined as the sum of TOC and inorganic carbon, TC was measured on unacidified, powdered samples using a Yanagomoto MT-2 carbon-hydrogen-nitrogen analyzer. The TOC content of the powdered sample was then analyzed following treatment with 1-N hydrochloric acid. The amount of inorganic carbon (taken as biogenic carbonate) was estimated by difference from the TC and TOC measurements:

$$CaCO_3\ (\text{wt\%}) = (\text{TC wt\%} - \text{TOC wt\%}) \times (100/12).$$

Opal percentages (Table 3) were estimated by smear-slide analysis from the sum of diatom, radiolarian, and sponge spicule percentages. Aluminosilicate content (Table 3) was estimated by difference: percent aluminosilicate = 100% – biogenic fractions (TOC, $CaCO_3$, and opal). Excess barium (Ba[ex]) determinations given in Table 3 are described below.

Major and Minor Element Concentration

Major and minor elements were measured on splits from each sample by X-ray fluorescence (XRF) using a Rigaku model 3270 XRF (Tables 4, 5). Samples were powdered for 10 min in a ball mill after drying overnight at 105°C. Fusion beads were then prepared from 0.4 ± 0.0002 g sediment mixed with 4 ± 0.002 g Li-tetraborate and held in a vinyl chloride ring for XRF analysis. Barium and the other minor elements were measured on a carbonate-free basis. Carbonate and organic carbon was removed from the powdered sediment by the addition of 4-M acetic acid (Hyun, 1997).

The reproducibility of these results between runs was tested by replicate analysis of standards with known elemental concentration and samples with unknown elemental concentrations. Analytical error for the major elements ranged from 1% to 5%. Representative duplicate experimental results for the minor elements are given in Table 6. Minor elements typically exhibit errors <1% on both standards and unknown samples. In the case of barium, errors did not exceed 1% on either standards or unknown samples and were independent of the measured Ba concentration.

Determination of Excess Barium (Ba[ex])

Although its formation mechanism is not well understood, non-matrix-bound Ba, sometimes called bio-Ba but referred to here as Ba(ex), has been used as a productivity proxy in a variety of oceanic settings (Schmitz, 1987; Bishop, 1988; Dehairs et al., 1980, 1990;

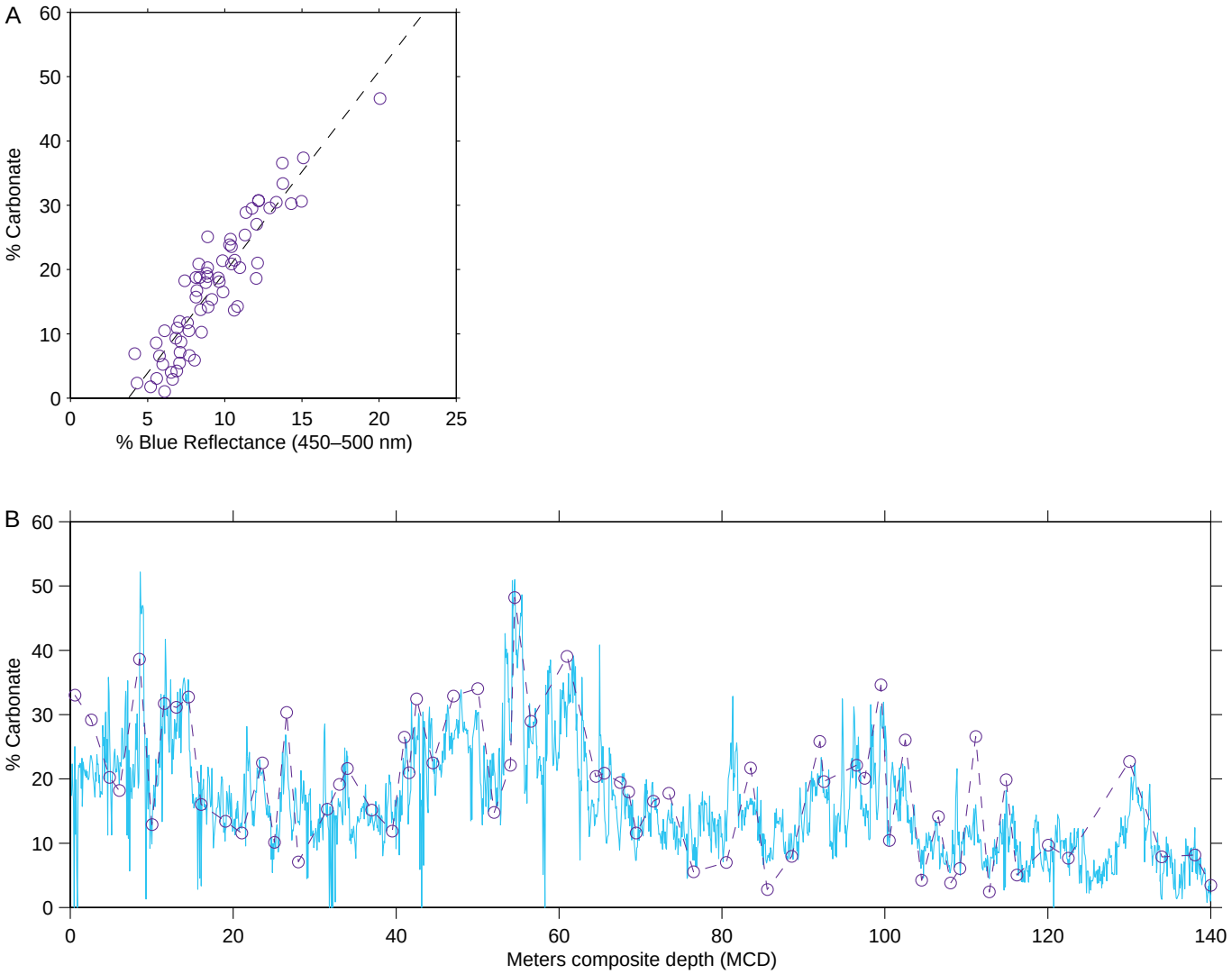

Figure 2. Percent blue reflectance characteristics for Site 983. **A.** Correlation between percent blue reflectance and percent carbonate for Site 983. **B.** Proxy percent carbonate derived from the Site 983 spliced reflectance record (solid gray line). Carbonate values from discrete samples are plotted for comparison (open circles connected by dotted lines). See "Methods and Materials" section for further details on calibration.

Dymond et al., 1992; François et al., 1995). The sedimentary sources of barium can be classified into five main components: (1) barite attached to discrete particles (Ba[ex], which is useful as a paleoproductivity proxy), (2) barium bound in biogenic carbonate, (3) barium bound in biogenic opal, (4) barium bound in organic matter, and (5) barium bound in aluminosilicates. The use of barium as a productivity proxy requires that total barium measurements be corrected for contributions from each of the bound barium forms listed above. In hemipelagic settings, most of the bulk sedimentary barium is clearly related to terrigenous aluminosilicate materials, making that form of barium the greatest likely source of error in Ba-based productivity estimates (Dymond et al., 1992). To estimate the amount of barite possibly related to total surface production, we used a modified version of the normative algorithm from Gingele and Dahmke (1994):

$$\mathrm{Ba(ex)} = \mathrm{Ba(total)} - \mathrm{Ba(bound\ component)},$$

$$\text{where Ba(bound component)} = (W_{ppm} \times \mathrm{CaCO_3\ wt\%}/100)$$

$$+ (X_{ppm} \times \text{opal\%}/100)$$

$$+ (Y_{ppm} \times \text{TOC wt\%}/100)$$

$$+ (Z_{ppm} \times \text{aluminosilicate\%}/100).$$

The weighting coefficients W, X, Y, and Z represent the average concentrations of barium in each bounding component. Gingele and Dahmke (1994) used values of W = 30 ppm for carbonate-bound Ba from Lea and Boyle (1989), X = 120 ppm for opal-bound Ba from Riley and Roth (1971), Y = 60 ppm for TOC-bound Ba from Martin and Knauer (1973), and Z = 400 ppm for terrigenous-bound Ba, although a value of 452 ppm from Taylor et al. (1964) may be more appropriate. The greatest source of potential error in Ba(ex) determinations thus arises from aluminosilicate-bound (and, to a lesser extent, opal-bound) barium resulting from their higher average Ba content than TOC or carbonate. Because Ba(total) is defined here on a carbonate-free and TOC-free basis, Ba(ex) was calculated using a simplified algorithm:

$$\mathrm{Ba(ex)} = \mathrm{Ba(total)} - (120\ \text{ppm} \times \text{opal\%}/100)$$

$$- (452\ \text{ppm} \times \text{aluminosilicate\%}/100).$$

Table 1. Age model for Site 983 sediments.

Depth (mcd)	Age (ka)	Linear sedimentation rate (cm/k.y.)
0.00	0.00	NA
3.57	12.58	28.38
3.81	21.94	2.56
7.68	70.82	7.92
13.12	118.69	11.36
15.79	128.31	27.76
19.50	171.37	8.62
21.25	188.29	10.34
21.97	193.18	14.72
22.98	200.57	13.67
23.80	215.54	5.48
26.95	240.19	12.78
27.66	244.18	7.79
31.30	288.50	8.21
31.96	297.00	7.77
33.39	307.00	14.30
34.84	318.00	13.18
37.88	331.00	23.39
38.68	339.00	10.00
44.26	395.00	9.96
50.75	420.00	25.96
55.80	481.00	8.28
57.20	497.00	8.75
61.48	524.00	15.85
67.43	571.00	12.66
72.39	610.00	12.72
74.89	625.00	16.67
82.18	692.00	10.88
85.62	722.00	11.47
87.62	750.00	7.14
90.66	780.00	10.13
117.24	990.00	12.66
131.83	1070.00	18.24
156.75	1230.00	15.58

Notes: All depth-age pairs are based on planktonic foraminiferal $\delta^{18}O$ stratigraphic picks from J. McManus (unpubl. data) and Channell et al. (1998), with the exception of the depth and age of the Brunhes/Matuyama boundary (780 ka), Jaramillo top (990 ka), Jaramillo bottom (1070 ka), and last occurrence of *Gephyrocapsa* spp. A/B (N) (1230 ka), which are used as reported in Jansen, Raymo, Blum, et al. (1996). NA = not available.

Excess barium determinations generated with this modified algorithm can be found in Table 3. Inclusion of the correction terms for carbonate-bound and TOC-bound barium would decrease the Ba(ex) estimates presented here by <7% on average, in all but five samples with Ba(ex) concentrations <20 ppm. In samples with Ba(ex) concentrations <20 ppm, the additional corrections would represent a significant fraction of the reported Ba(ex) values. Use of these additional correction factors would not, however, alter the structure of the downcore Ba(ex) record and thus do not affect the results presented here. Our approach is problematic in those sediments with very high terrigenous barium contributions or in which diagenetic barium remobilization has occurred (as discussed below). In the former case, 23 of the samples had estimates of terrigenous-bound barium that exceeded the measured barium content. It was thus not possible to estimate meaningful Ba(ex) values for these samples using this method.

Table 2. Sample intervals and ages of discrete samples, Site 983.

Hole	Core, section	Depth (mcd)	Age (ka)
A	1H-1	0.56	1.97
A	1H-2	2.56	9.02
A	1H-4	4.84	34.95
A	1H-5	6.02	49.85
C	2H-3	8.51	78.12
C	2H-4	10.01	91.32
C	2H-5	11.51	104.52
A	2H-3	13.05	118.07
A	2H-4	14.52	123.73
A	2H-5	16.05	131.33
B	3H-2	19.03	165.91
C	3H-2	21.04	186.26
C	3H-3	23.56	211.16
C	3H-5	25.06	225.40
C	3H-6	26.56	237.14
B	4H-2	28.00	248.32
C	4H-3	31.56	291.85
C	4H-4	33.06	304.69
C	4H-4	34.02	311.78
A	4H-5	37.02	327.32
A	4H-7	39.54	347.63
C	5H-2	41.02	362.48
C	5H-3	41.56	367.90
C	5H-3	42.52	377.54
A	5H-2	44.51	395.97
A	5H-4	47.03	405.67
A	5H-6	50.03	417.23
C	6H-2	52.04	435.58
C	6H-3	54.02	459.50
C	6H-4	54.56	466.02
C	6H-5	56.54	489.46
B	7H-3	61.00	520.98
C	7H-3	64.51	547.93
C	7H-4	65.53	555.99
C	7H-5	67.51	571.63
C	7H-6	68.53	579.65
C	7H-6	69.49	587.20
B	8H-3	71.57	603.55
C	8H-2	73.51	616.72
C	8H-4	76.51	639.89
B	9H-2	80.54	676.93
B	9H-4	83.54	703.86
C	9H-3	85.56	721.48
C	9H-5	88.56	763.16
B	10H-3	92.02	790.74
B	10H-3	92.50	794.54
C	10H-4	96.51	826.22
C	10H-5	97.53	834.28
C	10H-6	99.51	849.92
B	11H-2	100.53	857.98
B	11H-3	102.51	873.62
C	11H-2	104.52	889.50
C	11H-4	106.56	905.62
C	11H-5	108.06	917.47
C	11H-5	109.20	926.48
B	12H-2	111.15	941.88
B	12H-3	112.81	955.00
C	12H-2	114.87	971.28
C	12H-3	116.21	981.86
C	12H-6	120.07	1005.52
B	13H-2	122.49	1018.79
A	13H-5	130.01	1060.02
C	14H-2	134.01	1084.00
C	14H-4	138.05	1109.94
C	14H-6	140.02	1122.58

RESULTS

Sediment Composition and Lithologic Changes

Sediments at Site 983 vary in composition from ~10% to 50% biogenic material by weight. The primary biogenic component is calcium carbonate, which varies from 2.81 to 48.24 wt% with an average value of ~16 wt%. Biogenic silica content is highly variable, whereas TOC rarely exceeds 0.5 wt% (Table 3). The C/N weight ratio is commonly used to characterize various types of organic matter (Müller and Suess, 1979; Stein, 1990). The sediment C/N ratio at Site 983 is mostly <10, a typical marine value, which indicates no significant terrestrial component (Jansen, Raymo, Blum, et al., 1996). Thus, the organic carbon signature at this site can be interpreted to some extent as a marine organic productivity proxy. We also observe a strong correlation ($r^2 = 0.83$) between color reflectance and carbonate content (Fig. 2), consistent with results from Harris et al. (1997) and Ortiz et al. (Chap. 19, this volume).

Downcore concentrations of major elements (Fig. 3) indicate that the sediments exhibit fairly constant SiO_2 content, concordant with shipboard smear-slide observation (Jansen, Raymo, Blum, et al., 1996). At ~420-600 ka between 50 and 70 mcd, there is a significant geochemical shift in which the concentrations of most major and minor elements decrease (Fig. 3; Tables 4, 5). This difference in chemical composition between the upper and lower parts of the record probably results from differences in the supply of clastic material and a potential change in terrigenous provenance at ~600 ka. However, carbonate-free Th and K_2O covary throughout the record (arrows in Fig. 3). The molar Ti/Al ratio exhibits a strong inverse correlation with carbonate-free Th and K_2O ($r = –0.93$ relative to carbonate-free Th, $N = 65$). The timing of these cycles in terrigenous composition is

Table 3. Analytical results for total organic carbon, carbonate, biogenic opal, aluminosilicate, and Ba(ex) at Site 983.

Depth (mcd)	TOC (wt%)	$CaCO_3$ (wt%)	Opal (%)	Aluminosilicate (%)	Ba(ex)
0.56	0.64	33.02	6	60.34	183.40
2.56	0.69	29.19	3	67.12	238.90
4.84	0.29	20.21	1.5	78.00	205.00
6.02	0.30	18.16	0.7	80.84	220.40
8.51	0.23	38.65	1	60.12	285.20
10.01	0.36	12.9	1	85.74	53.60
11.51	0.27	31.73	2	66.00	167.90
13.05	0.28	31.11	0.7	67.91	195.00
14.52	0.38	32.69	1	65.93	84.60
16.05	0.33	16.04	1.5	82.13	106.90
19.03	0.30	13.4	2	84.30	82.60
21.04	0.20	11.56	8	80.24	
23.56	0.30	22.51	12	65.19	134.70
25.06	0.26	10.14	10	79.60	
26.56	0.27	30.31	10	59.42	106.00
28.00	0.22	7.11	3.3	89.37	24.90
31.56	0.20	15.27	7	77.53	
33.06	0.22	19.17	7	73.61	
34.02	0.24	21.61	0	78.15	
37.02	0.25	15.13	3	81.62	59.60
39.54	0.29	11.9	2	85.81	
41.02	0.32	26.52	4	69.16	69.30
41.56	0.27	20.93	3	75.80	13.00
42.52	0.31	32.46	3	64.23	
44.51	0.19	22.47	3	74.34	192.90
47.03	0.40	32.9	3	63.70	142.20
50.03	0.65	34.05	3	62.30	143.10
52.04	0.20	14.79	2	83.01	7.20
54.02	0.21	22.13	3	74.66	
54.56	0.30	48.24	1.5	49.96	136.40
56.54	0.35	28.95	2	68.70	84.80
61.00	0.46	39.07	6	54.47	21.30
64.51	0.29	20.36	3	76.35	
65.53	0.36	20.87	3	75.77	12.00
67.51	0.22	19.45	3	77.33	33.50
68.53	0.24	17.99	3	78.77	70.00
69.49	0.21	11.62	3	85.17	
71.57	0.22	16.55	10	73.23	284.30
73.51	0.37	17.75	9	72.88	236.00
76.51	0.24	5.56	8	86.20	
80.54	0.28	7.02	15	77.70	84.80
83.54	0.27	21.72	12	66.01	77.10
85.56	0.33	2.81	7	89.86	
88.56	0.15	7.95	7	84.90	39.00
92.02	0.36	25.83	1.5	72.31	87.60
92.50	0.27	19.61	2	78.12	41.10
96.51	0.13	22.13	3	74.74	
97.53	0.24	20.08	3	76.68	
99.51	0.23	34.6	3	62.17	130.80
100.53	0.21	10.43	2.5	86.86	193.50
102.51	0.45	26.07	2.5	70.98	108.60
104.52	0.23	4.22	3	92.55	
106.56	0.40	14.1	3	82.50	85.50
108.06	0.12	3.78	3	93.10	
109.20	0.14	6.02	3	90.84	2.10
111.15	0.28	26.58	2	71.14	76.90
112.81	0.12	2.41	2.5	94.97	
114.87	0.20	19.85	3	76.95	5.90
116.21	0.19	5.05	3	91.76	28.70
120.07	0.20	9.68	3	87.12	
122.49	0.21	7.69	2	90.10	
130.01	0.34	22.73	5	71.93	
134.01	0.17	7.88	3	88.95	
138.05	0.28	8.19	0	91.53	
140.02	0.21	3.48	3	93.31	

Notes: Opal contents are derived from smear-slide data. Diatoms, radiolarians, and sponge spicule contents were added and interpolated. Aluminosilicate contents were calculated by 100% –biogenic fractions (TOC, $CaCO_3$, and opal). Ba(ex) was calculated using the modified algorithm of Gingele and Dahmke (1994). Blank entries for Ba(ex) indicate negative concentrations resulting from inappropriate aluminosilicate Ba content or no measurement.

linked to the major Northern Hemisphere glacial–interglacial cycles (Fig. 3).

The strong inverse correlation between the molar Ti/Al ratio and carbonate-free Th implies that the terrigenous material at this site is derived from two components. This can be seen clearly in plots of the molar Ti/Al ratio vs. carbonate-free Th (Fig. 4A) or TiO_2 vs. Al_2O_3 (Fig. 4B). Estimates of the geochemical composition of potential end-members including continental terrigenous material (based on an average of continental shield sample [Taylor and McLennan, 1985]), nonrhyolitic, Icelandic basalt (C. Langmuir, pers. comm., 1998), high-Ti suite basalts of the southwest Faeroe Islands (Waagstein, 1988), and red-bed clays from the Iceland-Faeroe Ridge (Parra et al., 1986) are plotted in Figure 4A and 4B for comparison with data from the Site 983 sediments. These data indicate that the Site 983 sediments are derived from a mixture of a continental IRD component (low Ti, high Al, and high Th) and an oceanic, basaltic component (high Ti, high Al, and low Th). Biogenic particulates ($CaCO_3$ and opal), which are low in Ti and Al in comparison to the terrigenous material, act to some extent as a diluent (Fig. 4B).

The location of Site 983 and the high sediment TiO_2 content suggest the Icelandic basalt as a potential source of the oceanic end-member. However, the TiO_2 content of these sediments and their molar Ti/Al ratio exceed that of Icelandic basalt. Because the TiO_2 and Al_2O_3 contents of basalt are not easily altered during mechanical or physical weathering (Gislason et al., 1996), alteration cannot explain this discrepancy. The Al_2O_3 and TiO_2 contents of the most enriched samples from Site 983 (Fig. 4B) lie between those of Icelandic and high-Ti suite basalt from the southwest Faeroe Islands, which were formed during an earlier phase of Icelandic hot spot volcanism (Waagstein, 1988). The intermediate behavior of the Site 983 sediments between these two oceanic components is also clear from the molar Ti/Al ratio and carbonate-free Th content of the sediments (Fig. 4A). The sediments of the Gardar Drift are thus not derived solely from eroded Icelandic basalt as hypothesized by Ruddiman and Bowles (1976) but must contain a significant contribution of basalt eroded from the Faeroe Islands as well. The fact that this material is derived from a mixture of Icelandic and Faeroe Island basalt precludes us from quantitatively separating the terrigenous sediments at Site 983 by mass balance because the exact chemical composition of this complex basaltic end-member is not currently well known. This is unfortunate because such a procedure might have provided a better means of correcting for terrigenous Ba content, allowing us to generate improved Ba(ex) estimates.

The most likely means of transporting material from the Faeroe Islands to the Gardar Drift is as fine-grained particles carried by the ISOW. The extremely high TiO_2 content and molar Ti/Al ratio of the Iceland-Faeroe Ridge red-bed clays (~0.6) suggest that they have not contributed significantly to the sediments of the Gardar Drift during the past million years. During glacial periods, the dominant terrigenous component deposited on the Gardar drift is poorly sorted IRD, whereas during interglacial periods, fine-grained basaltic material supplied by bottom currents dominates. Our data provide longer records with significantly better age control than the data of Ruddiman and Bowles (1976) and Grousset et al. (1982), who observed similar glacial–interglacial variability in the terrigenous composition of North Atlantic sediments. Consistent with this interpretation, glacial–interglacial cycles in clay mineralogy have recently been reported for nearby core SU 90-33 and at other North Atlantic sites (Bout-Roumazeilles et al., 1997).

DISCUSSION

Variations of Ba(ex) and Diagenetic Remobilization

Apart from barite-phase barium, aluminosilicate-related barium and various biogenic-bound forms of barium may contribute significantly to the total sediment barium content, especially in nearshore and shallow-water environments (Dymond, 1981). The accumulation rate of sedimentary barium thus depends not only on biogenic surface-water productivity but also on dissolved barium concentration in the water column and the depth of sediment deposition. In addition, anoxic mobilization and hydrothermal activity have been known to produce relatively high levels of authigenic barium unrelated to surface bioproductivity (von Breymann et al., 1990; Torres et al., 1996).

Table 4. Bulk major element concentrations.

Depth (mcd)	SiO_2 (%)	TiO_2 (%)	Al_2O_3 (%)	Fe_2O_3 (%)	MnO (%)	MgO (%)	CaO (%)	Na_2O (%)	K_2O (%)	P_2O_5 (%)	LOI (%)
0.56	42.95	1.76	10.20	9.51	0.14	3.78	26.52	3.86	0.93	0.25	17.89
2.56	45.13	1.58	11.30	9.14	0.17	3.86	23.91	3.45	1.16	0.23	17.13
4.84	53.26	1.32	13.67	8.04	0.13	3.65	14.42	3.23	2.24	0.19	13.00
6.02	54.29	1.23	14.87	8.37	0.13	3.64	13.10	3.19	2.09	0.19	13.02
8.51	39.81	1.23	10.04	8.49	0.18	3.39	30.20	3.77	1.66	0.22	20.44
10.01	52.71	1.87	13.87	10.76	0.16	4.56	12.22	3.40	1.44	0.24	10.25
11.51	44.34	1.71	11.22	9.44	0.19	3.93	25.49	3.45	0.94	0.24	17.01
13.05	43.68	1.75	10.57	10.13	0.20	3.82	25.96	3.42	0.84	0.29	17.47
14.52	46.72	1.46	10.79	8.38	0.19	3.51	25.93	2.93	0.95	0.23	17.80
16.05	53.21	1.39	14.92	9.37	0.14	4.03	12.39	3.10	2.22	0.21	12.36
19.03	52.55	1.63	14.65	10.35	0.15	4.37	11.58	3.44	2.05	0.24	11.68
21.04	52.17	2.02	13.93	10.99	0.17	4.46	12.20	3.40	1.48	0.26	9.23
23.56	48.06	1.76	11.65	10.07	0.21	4.07	19.90	3.57	1.09	0.26	13.60
25.06	53.52	2.00	14.38	10.65	0.16	4.54	11.18	3.22	1.63	0.23	8.58
26.56	45.11	1.58	11.07	9.11	0.26	3.80	25.21	3.26	1.06	0.26	16.84
28.00	56.75	1.50	15.28	10.48	0.13	4.22	6.70	3.63	2.54	0.21	8.90
31.56	50.46	1.93	13.36	10.68	0.18	4.52	14.54	3.62	1.49	0.24	10.88
33.06	45.96	1.94	11.81	11.97	0.21	4.03	18.01	3.22	1.25	0.28	10.00
34.02	47.12	1.80	12.30	10.63	0.22	4.02	18.93	3.82	1.32	0.26	12.80
37.02	53.74	1.82	12.72	9.73	0.17	4.00	14.67	3.00	1.34	0.22	10.40
39.54	55.12	1.54	15.77	9.68	0.11	3.92	10.08	2.97	2.19	0.21	10.13
41.02	45.60	1.66	12.41	10.00	0.19	3.80	22.50	3.10	1.12	0.26	16.02
41.56	48.52	1.79	13.18	10.00	0.17	4.06	18.00	3.22	1.37	0.31	13.25
42.52	42.36	1.71	10.54	9.61	0.23	3.53	28.48	2.97	0.73	0.30	17.70
44.51	46.57	1.88	11.97	10.37	0.16	3.80	20.12	3.52	1.13	0.28	13.46
47.03	44.51	1.57	10.43	8.41	0.16	3.19	28.15	2.91	0.91	0.25	18.07
50.03	43.36	1.35	11.44	8.12	0.19	3.30	28.83	2.74	0.84	0.24	19.99
52.04	51.28	1.68	14.97	10.47	0.13	4.00	12.94	3.10	1.95	0.25	11.89
54.02	48.60	1.70	12.95	9.65	0.15	3.81	19.00	3.03	1.27	0.24	13.31
54.56	33.55	1.31	8.48	7.80	0.23	2.91	42.08	2.47	0.66	0.31	24.50
56.54	46.43	1.52	11.43	8.76	0.14	3.38	24.38	2.89	1.04	0.23	15.88
61.00	41.77	1.38	9.26	7.59	0.16	2.98	33.06	2.73	0.82	0.23	20.21
64.51	48.15	1.82	12.94	10.86	0.18	4.15	17.82	3.23	1.28	0.27	12.65
65.53	48.43	1.79	11.77	10.34	0.19	3.89	18.90	3.42	1.21	0.25	13.16
67.51	47.57	2.06	12.10	11.19	0.20	4.10	18.09	3.47	1.11	0.29	11.93
68.53	50.03	1.93	12.51	10.57	0.19	4.13	16.91	3.08	1.17	0.24	11.44
69.49	50.14	2.23	13.36	12.12	0.19	4.52	13.30	3.41	1.15	0.34	8.47
71.57	51.58	1.80	12.70	10.58	0.18	4.06	15.52	3.28	1.38	0.24	12.03
73.51	51.61	1.73	12.96	9.87	0.21	3.92	15.92	3.03	1.45	0.25	12.12
76.51	55.56	1.68	16.04	10.78	0.13	4.41	6.21	3.44	2.47	0.23	7.68
80.54	56.67	1.78	15.22	10.07	0.13	4.02	7.50	3.30	2.19	0.21	7.52
83.54	49.38	1.77	11.64	9.98	0.19	3.82	19.20	3.04	1.13	0.26	13.29
85.56	57.95	1.80	15.37	10.60	0.11	0.11	4.11	4.87	3.38	2.26	5.44
88.56	54.18	1.88	15.09	11.08	0.14	4.51	8.58	3.41	2.03	0.25	7.96
92.02	46.74	1.69	11.31	9.75	0.20	3.79	22.68	2.86	0.95	0.25	14.82
92.50	51.63	1.64	12.63	9.42	0.16	3.92	17.32	2.80	1.23	0.21	12.42
96.51	45.88	1.85	11.43	11.08	0.20	3.88	19.77	3.68	1.22	0.33	12.85
97.53	48.01	2.07	12.05	11.13	0.20	4.08	19.01	3.01	1.02	0.31	12.55
99.51	43.05	1.50	9.99	8.94	0.27	3.48	29.00	2.97	0.88	0.30	18.37
100.53	53.02	1.82	13.64	11.88	0.14	4.28	10.82	3.34	1.80	0.23	9.25
102.51	48.27	1.51	11.29	8.95	0.20	3.68	22.37	2.81	0.99	0.21	14.98
104.52	56.03	1.96	15.32	11.01	0.13	4.35	6.64	3.52	1.97	0.24	5.84
106.56	54.25	1.62	14.92	9.70	0.13	3.83	11.76	2.88	1.91	0.21	10.92
108.06	54.80	2.19	14.18	11.80	0.16	4.60	8.12	3.46	1.62	0.23	4.53
109.20	51.89	2.13	12.85	12.78	0.15	4.26	9.32	3.94	1.69	0.23	6.25
111.15	47.28	1.74	10.72	9.49	0.23	3.77	23.24	2.81	0.89	0.24	14.83
112.81	53.67	2.22	13.89	13.52	0.14	4.80	6.79	4.01	1.81	0.28	5.67
114.87	49.02	1.89	12.05	10.47	0.27	4.09	18.50	2.98	1.02	0.29	12.45
116.21	59.20	1.60	14.93	9.73	0.11	3.90	6.14	3.23	2.23	0.18	6.63
120.07	52.53	1.99	14.29	11.42	0.19	4.57	11.05	3.12	1.57	0.27	8.07
122.49	52.76	2.09	13.83	11.95	0.17	4.53	10.40	3.59	1.53	0.27	7.59
130.01	47.52	1.91	11.45	10.17	0.23	3.81	21.13	3.22	0.96	0.27	13.97
134.01	50.98	2.09	12.92	12.71	0.19	4.76	11.65	3.08	1.14	0.24	4.72
138.05	54.33	1.83	14.39	10.99	0.21	4.36	9.59	3.37	1.81	0.27	8.75
140.02	53.50	2.19	14.78	12.24	0.17	4.99	7.70	3.38	1.65	0.28	5.22

Note: LOI = loss on ignition.

Understanding the diagenetic mobilization of sedimentary barium is thus essential for the application of excess barium as a paleoproductivity proxy. In this study, the degree of diagenetic mobilization was evaluated by two methods. First, we checked the interstitial-water sulfate ion concentration at Site 983 (Fig. 5). In anoxic sediments, the associated decrease in pore-water sulfate concentration leads to enhanced dissolution of barite and remobilization under sulfate-reducing conditions (von Breymann et al., 1992). Intense diagenetic remobilization under sulfate-reducing conditions can lead to the production of a barite front (e.g., Torres et al., 1996) or to significant increases in dissolved barium within the sulfate reduction zone (von Breymann et al., 1990). At Site 983, in sediments deeper than ~90 meters below seafloor (mbsf) or ~100 mcd, sulfate ion concentration is extremely low, ranging only from 0 to 0.2 mM (Jansen, Raymo, Blum, et al., 1996). This extremely low pore-water sulfate ion concentration is sufficient to foster remobilization of sedimentary barium and thus compromises the usefulness of Ba(ex) as a paleoproductivity proxy below 100 mcd at this site. Pore-water barium content was not measured during Leg 162, and our relatively coarse sampling resolution is not sufficient to precisely define the location of the barite front, although a peak in total Ba (589 ppm) at 100 mcd is consistent with the pore-water sulfate data and thus may be associated with the barite front.

As a second test of Ba remobilization, we compared the downcore, carbonate-free, Ba profile with those of several major and minor elements as potential indicators of diagenetic influence. For example, variations in Mn concentration can indicate the initiation of diagenetic processes that may be associated with Ba remobilization (Frol-

Table 5. Carbonate-free minor element concentrations.

Depth (mcd)	Ba (ppm)	Nb (ppm)	Ni (ppm)	Pb (ppm)	Rb (ppm)	Sr (ppm)	Th (ppm)	Y (ppm)	Zr (ppm)
0.56	463.34	18.38	37.23	6.66	35.28	253.48	3.36	28.16	200.72
2.56	545.88	18.10	45.96	11.37	59.79	236.22	4.63	28.69	208.60
4.84	559.38	18.30	24.78	9.24	105.42	134.49	6.77	18.08	234.90
6.02	586.58	15.03	49.14	13.75	115.73	175.53	8.76	24.44	195.58
8.51	558.10	16.45	47.53	10.72	77.60	204.40	5.70	27.34	197.67
10.01	442.37	16.02	48.52	8.36	61.08	222.68	5.40	27.90	204.91
11.51	468.60	15.30	47.80	9.08	48.30	246.33	4.44	27.95	185.55
13.05	502.81	18.09	43.76	23.10	36.64	274.64	4.05	33.79	211.80
14.52	383.80	19.91	26.93	5.27	61.63	163.60	4.49	20.82	251.45
16.05	479.86	16.04	50.19	15.91	110.49	158.14	8.78	26.58	206.60
19.03	466.01	17.22	48.65	14.21	88.09	181.52	6.64	25.17	202.89
21.04	351.55	21.03	30.94	5.15	55.05	179.56	4.20	20.29	240.86
23.56	443.74	18.63	43.27	9.06	45.17	227.74	4.75	30.42	211.03
25.06	256.43	19.97	27.04	4.78	62.82	166.75	4.68	19.53	238.50
26.56	386.56	18.16	33.32	5.46	54.86	168.93	4.98	18.06	213.56
28.00	432.80	15.78	43.84	13.92	97.51	151.67	7.42	25.20	201.62
31.56	339.88	17.19	46.81	8.95	57.49	200.69	4.90	25.62	203.51
33.06	311.86	17.54	43.63	4.91	34.15	226.83	3.33	30.28	211.09
37.02	432.19	16.20	42.41	8.39	49.18	234.16	4.21	26.45	206.45
39.54	365.37	18.31	31.58	11.30	104.76	141.55	7.00	19.98	228.49
41.02	386.72	17.78	45.33	10.92	60.34	226.82	4.87	33.26	217.58
41.56	359.19	18.94	48.20	9.03	61.04	246.53	5.29	31.37	215.39
42.52	287.80	19.46	33.99	4.60	36.47	212.07	3.49	24.93	220.77
44.51	532.53	19.36	43.86	6.57	42.27	262.33	3.70	32.75	224.28
47.03	433.71	21.28	37.51	7.11	43.94	255.94	4.20	34.99	250.50
50.03	428.30	16.98	44.72	11.73	71.63	180.56	6.08	21.10	196.21
52.04	384.86	17.92	49.51	21.42	87.99	213.91	7.62	27.55	205.98
54.02	272.83	18.49	41.67	6.84	65.84	184.91	5.03	19.21	211.56
54.56	364.03	19.00	41.74	8.05	32.95	297.09	2.74	36.58	212.14
56.54	397.76	16.56	41.80	9.26	52.73	241.78	4.37	28.11	195.45
61.00	467.75	16.92	38.74	9.26	44.92	251.52	3.62	29.32	194.68
64.51	289.54	17.31	48.59	8.12	51.33	250.78	4.32	31.93	206.20
65.53	358.08	20.86	40.45	8.10	40.25	214.54	3.48	28.72	220.95
67.51	386.67	19.04	41.00	6.65	27.84	278.75	2.88	30.15	201.95
68.53	429.62	16.94	44.58	8.82	43.49	223.61	3.98	25.88	200.38
69.49	304.00	18.28	42.19	4.88	30.18	262.45	3.53	32.01	206.24
71.57	627.25	17.25	33.44	5.43	50.91	182.74	4.03	17.51	207.47
73.51	576.30	17.70	41.20	9.41	53.43	235.53	4.68	30.41	209.75
76.51	359.68	16.50	46.85	13.54	92.48	168.22	7.74	26.06	201.34
80.54	453.98	17.82	47.70	11.55	78.87	193.86	5.80	27.47	228.90
83.54	389.91	16.64	39.91	7.98	44.12	247.96	4.13	29.18	197.47
85.56	398.93	17.08	28.75	7.30	79.53	160.36	5.47	18.83	229.90
88.56	431.16	17.10	49.83	11.43	72.53	707.96	5.68	28.17	202.43
92.02	416.30	15.92	40.77	7.50	43.54	184.08	3.93	19.87	182.76
92.50	396.63	14.93	47.01	10.21	59.68	233.70	4.87	26.17	188.18
96.51	333.10	15.57	53.23	5.66	31.70	253.84	2.73	32.44	190.96
97.53	262.57	16.10	41.16	5.42	27.99	263.60	2.47	30.68	185.86
99.51	415.44	20.14	39.57	7.16	37.87	189.31	3.94	23.77	210.60
100.53	589.16	16.09	44.44	8.47	57.55	219.75	4.80	27.69	199.69
102.51	432.41	13.99	48.75	8.48	48.40	233.52	4.16	25.63	185.46
104.52	366.74	16.31	43.90	9.07	62.73	190.79	5.53	29.26	200.62
106.56	462.02	15.23	45.89	12.67	81.18	185.50	6.87	26.23	201.43
108.06	182.85	30.45	26.91	4.69	43.57	166.90	4.59	26.18	312.33
109.20	416.29	16.06	56.14	5.36	34.40	202.22	3.17	28.09	187.50
111.15	400.83	16.19	44.75	6.41	33.06	253.93	3.77	28.80	191.23
112.81	258.25	16.61	40.17	4.54	35.16	200.73	2.85	27.08	190.33
114.87	357.33	15.93	43.12	5.70	35.94	256.62	3.09	28.25	189.01
116.21	447.00	14.65	43.94	12.08	77.71	182.40	6.21	25.94	213.60
120.07	301.11	16.39	48.02	6.81	52.90	230.56	4.04	29.86	204.74
122.49	346.82	15.93	40.51	6.05	37.53	222.40	3.28	30.88	198.49
130.01	201.84	19.76	33.76	4.08	21.73	192.92	2.75	22.03	204.93
134.01	235.68	13.60	44.25	3.68	23.66	205.87	2.04	25.71	162.21
140.02	219.59	20.14	28.12	4.28	48.03	162.89	3.28	18.20	238.13

Table 6. Examples of the results of duplicate analyses (standard and unknown samples).

Element	HM-22.2 (standard)		UAP-349 (standard)		IZ-19 (standard)		Unknown	
	Series A	Series B	Series A	Series B	Series A	Series B	Series A	Series B
Ba	1471.80	1468.78	539.29	540.34	58.71	58.59	304.96	301.11
Nb	161.90	162.11	58.35	58.38	0.67	0.64	16.45	16.39
Ni	78.61	78.55	99.17	99.09	60.68	60.63	47.37	48.01
Pb	9.13	9.03	5.57	5.45	0.77	0.64	7.10	6.80
Rb	63.65	63.76	162.06	162.24	0.30	0.26	53.01	52.89
Sr	2268.23	2270.69	805.26	807.70	354.37	354.76	231.20	230.56
Th	22.87	23.04	8.70	8.82	0.67	0.73	4.31	4.03
Y	50.25	49.95	23.51	23.34	16.19	16.15	30.22	29.85
Zr	374.78	372.33	297.94	296.33	62.25	62.40	206.22	204.73

Note: Concentrations expressed in parts per million.

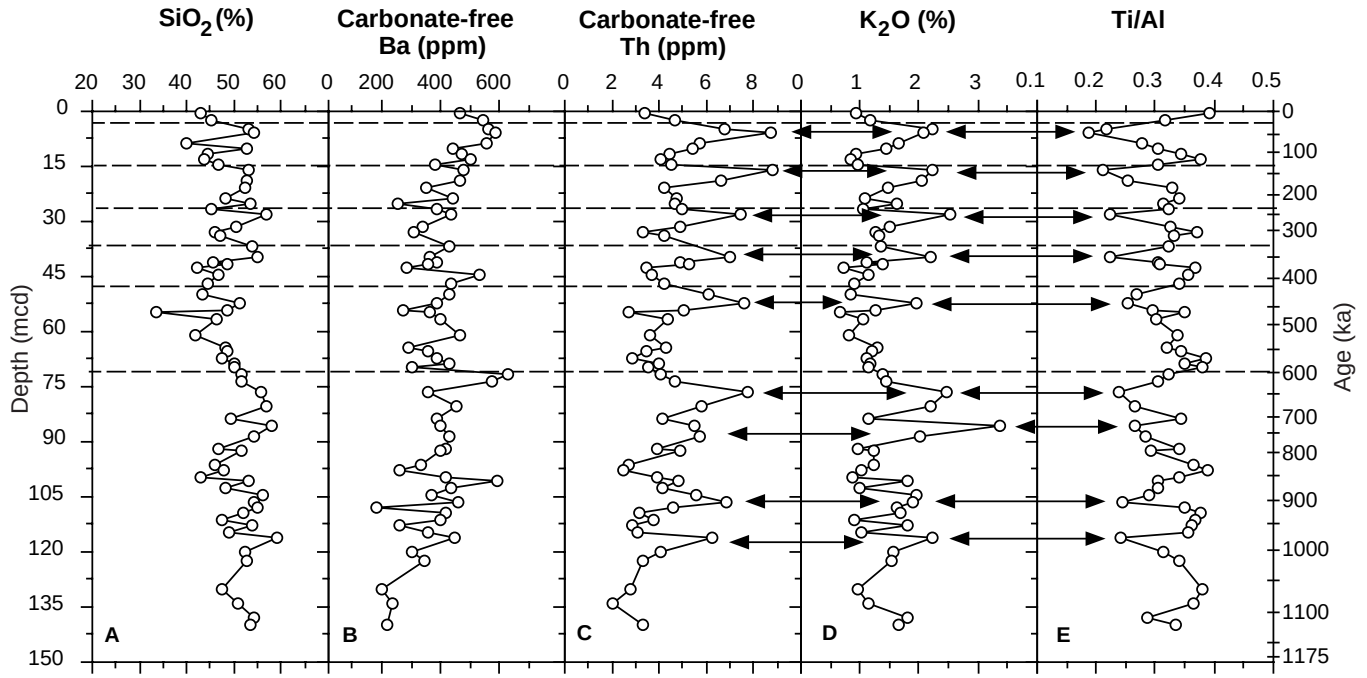

Figure 3. Profiles of **(A)** SiO_2, **(B)** carbonate-free Ba, **(C)** carbonate-free Th, **(D)** K_2O, and **(E)** the molar Ti/Al ratio for Site 983. Horizontal dashed lines mark the age of the major glacial terminations for reference. Horizontal arrows indicate correlated peaks and troughs between carbonate-free Th, K_2O, and the molar Ti/Al ratio.

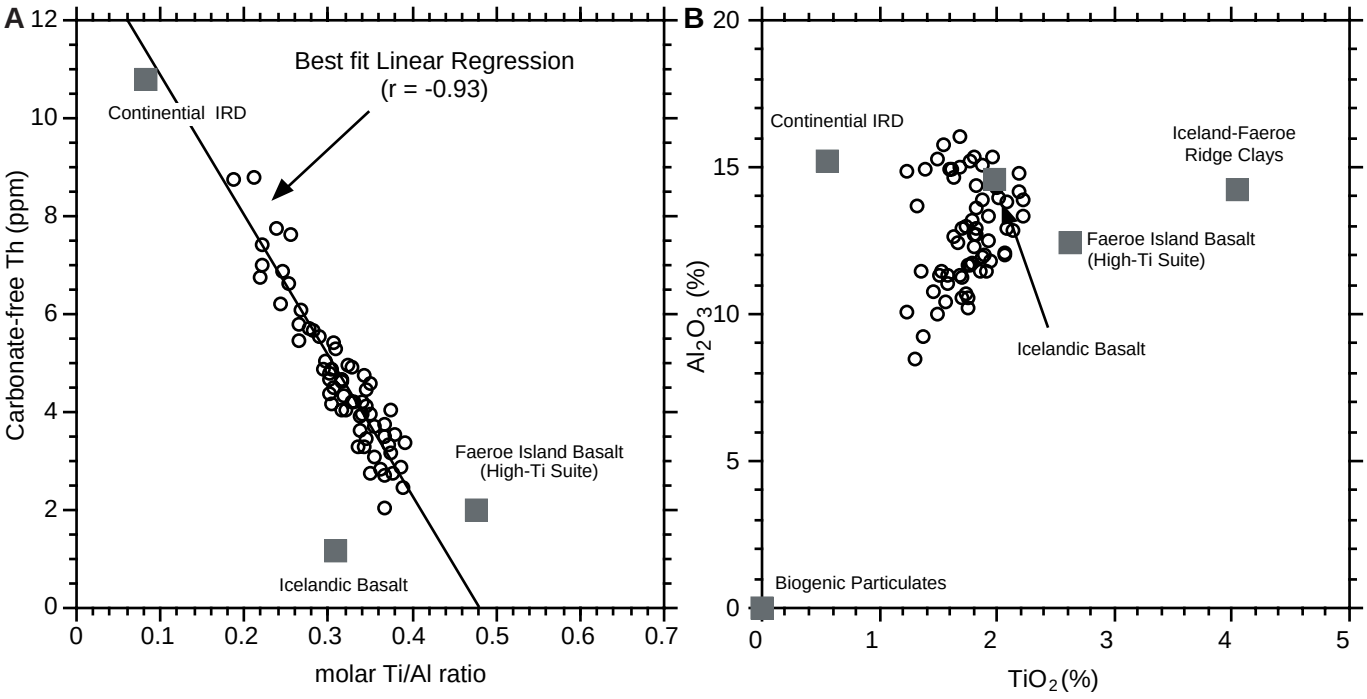

Figure 4. **(A)** Molar Ti/Al ratio vs. carbonate-free Th and **(B)** TiO_2 vs. Al_2O_3 for sediments for Site 983. The terrigenous material in these sediments is derived from two components: continental IRD and oceanic basalt. Continental end-member composition is from Taylor and McLennan (1985). Icelandic basalt end-member composition is from C. Langmuir (unpubl. data). Faeroe Island Basalt end-member composition is from Waagstein (1988), and Iceland-Faeroe Ridge clay composition is from Parra et al. (1986).

ich et al., 1979; von Breymann et al., 1992). The concordant variation of MnO (%) and carbonate-free barium below 100 mcd at Site 983 (Tables 4, 5) provides some additional evidence for the presence of remobilized Ba, although the complexity of the pore-water Mn cycle does not make this result entirely conclusive. Because of the possibility of Ba remobilization below 100 mcd at Site 983, Ba(ex) below that depth cannot be trusted as a reliable paleoproductivity proxy.

Low-Frequency Lithologic Variations at Site 983

The use of a variety of paleoproductivity proxies is advisable in most cases as each proxy is subject to different postdepositional changes. For this reason, we have used Ba(ex), TOC, and $CaCO_3$ (by direct measurement and through reflectance-based proxy estimates) to explore the low-frequency lithologic variability at Site 983. These carbonate variations, which occur on time scales spanning several glacial–interglacial cycles, could result from long-term changes in oceanic productivity, dissolution, and/or dilution by fine-grained terrigenous material carried to the site by ISOW.

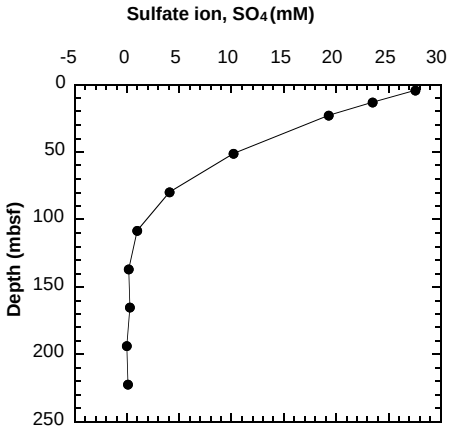

Figure 5. Interstitial-water sulfate ion concentration for Site 983. The sulfate ion concentration shows a systematic decrease, reaching essentially zero concentration at ~100 mbsf.

Although we have not directly assessed the effects of dissolution as part of this study, there is evidence to indicate that dissolution at this site is likely to be of relatively minor importance. Site 983 was drilled in 1983 m water depth on the Gardar Drift (Fig. 1). Today, this site is bathed by ISOW. This component of lower North Atlantic Deep Water extends to depths of at least 2400 m in this region of the North Atlantic (Oppo and Lehman, 1993). More corrosive southern source waters are thus situated well below Site 983 during the Holocene, and presumably during similar interglacial periods as well. However, during the last glacial maximum, a strong gradient between Glacial North Atlantic Intermediate Water and southern source water existed near the depth of this site (Oppo and Lehman, 1993). It is possible that dissolution occurred during glacial periods at Site 983, but visual observations of glacial foraminiferal shells from this site show no obvious signs of this.

Another possible source of carbonate variability at this site, dilution by fine-grained material, may be of some significance and deserves further attention. To account for potential dilution of sediment carbonate content by fine-grained terrigenous material, we calculated sediment mass-accumulation rates using the detailed age model described in a previous section (Fig. 6). SCAT reflectance values provide a high-resolution signal for comparison with the discrete carbonate samples (Fig. 6D). This comparison demonstrates that the discrete samples capture the full range of the low-frequency variability in these sediments. These calculations demonstrate that the total mass-accumulation rate for the past 1.2 m.y. at Site 983 has been dominated by the aluminosilicate flux to this site (Fig. 6B, C). The overall pattern of aluminosilicate mass-accumulation rate is characterized by a long-term decrease from 1200 to ~480 ka, followed by high values that once again gradually decrease toward the Last Glacial Maximum. This pattern differs considerably from that of the carbonate mass-accumulation rate (Fig. 6D), TOC mass-accumulation rate (Fig. 6E), and to some extent the Ba(ex) mass-accumulation rate (Fig. 6F). Mass-accumulation rates of the biogenic constituents are punctuated by high accumulation–rate events superimposed on a constant background. We visually estimate that these "events," which are best

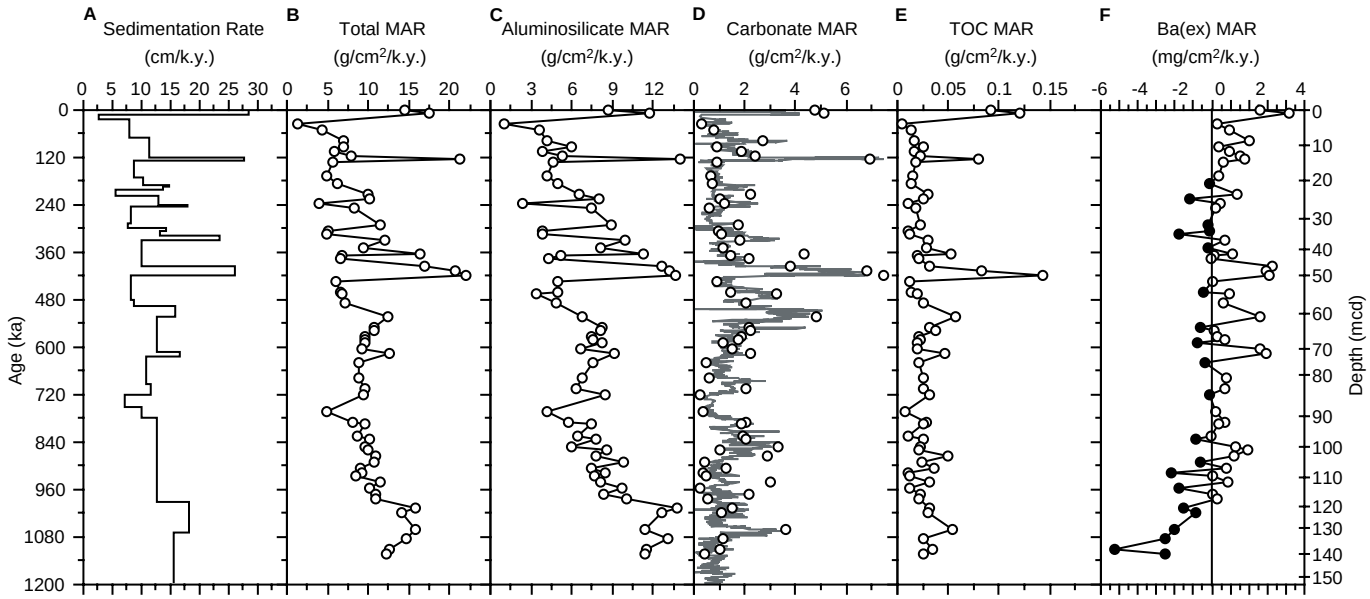

Figure 6. Profiles of **(A)** linear sedimentation rate, **(B)** total mass-accumulation rate (MAR), **(C)** aluminosilicate MAR, **(D)** $CaCO_3$ MAR, **(E)** total organic carbon (TOC) MAR, and **(F)** Ba(ex) MAR for Site 983. $CaCO_3$ MAR was estimated using reflectance-based proxy carbonate (solid line, 5D) and from discrete samples (open circles, 5D). Negative Ba(ex) MAR values (solid circles, 5F) indicate a failure of the Ba(ex) normative approach resulting from an overestimation of terrigenous barium, or Ba remobilization, because of sulfide reduction.

characterized in the carbonate mass-accumulation rate data, have durations of ~200 k.y. and are composed of bundles of glacial–interglacial cycles. Their timing does not seem to be defined by the occurrence of major stratigraphic boundaries such as the Brunhes/Matuyama boundary or the transition from the 40- to the 100-k.y. world (Raymo et al., 1997).

If terrigenous dilution were the dominant cause for the low-frequency variability in the biogenic mass-accumulation rates (MARs), we would expect to see an inverse correlation between the aluminosilicate MAR and that of the biogenic components (i.e., TOC, $CaCO_3$, and Ba[ex]). In contrast, we observe weak positive correlation with r^2 values ranging from 0.18 to 0.40 between the aluminosilicate and the biogenic MARs (Fig. 7A, C, E). These positive correlations may indicate greater preservation of biogenic constituents in high accumulation–rate sediments. In contrast to the weak correlations between aluminosilicate and biogenic MARs, we observed stronger correlations (r^2 values ranging from 0.54 to 0.70) between the MARs of the biogenic components (Fig. 7B, D, F). Because the aluminosilicate mass-accumulation-rate pattern is not strongly correlated with the MARs for TOC, $CaCO_3$, or Ba(ex), we infer that carbonate dilution is not the primary cause of the low-frequency variations in sedimentary carbonate content at this site. The stronger positive correlations between the biogenic MARs suggest that variations in oceanic production play a more important role in the low-frequency variability we observed.

To summarize, the carbonate-free Th, TiO_2, and Al_2O_3 data we present express a long-term cyclicity that is linked to glacial–interglacial cycles. This relationship suggests that these chemical constituents and the molar Ti/Al ratio in these sediments provide useful fingerprints at this site of continentally derived IRD (which dominates during glacial periods) and fine-grained basaltic material carried by the ISOW (which dominates during interglacial periods). Although estimates of Ba(ex) were difficult to make in some of these sediments because of either high aluminosilicate composition from mixed terrigenous sources or diagenetic Ba remobilization at depth, we are encouraged by the positive correlation between TOC, $CaCO_3$, and Ba(ex). This correlation suggests that Ba(ex) does carry information regarding paleoproductivity at these sites. The stronger positive correlations between the biogenic MARs than with the aluminosilicate MARs imply that variations in oceanic production play a role in the low-frequency variability at Site 983.

CONCLUSIONS

Major and minor elemental concentrations, total organic carbon, and Ba(ex) were investigated to evaluate the long-term lithologic variability at Site 983 and to evaluate the factors contributing to low-frequency carbonate variations first observed by sediment spectral reflectance. We observed cyclic variations in the concentration of carbonate-free Th, K_2O, and the sediment Ti/Al ratio. These cycles represent mixing between continental and oceanic basaltic terrigenous sources. The timing of these cycles matches that of the major glacial–interglacial cycles, which suggests that the cycles result from the supply of continental material IRD during glacial periods and fine-grained basaltic material by bottom currents during interglacial

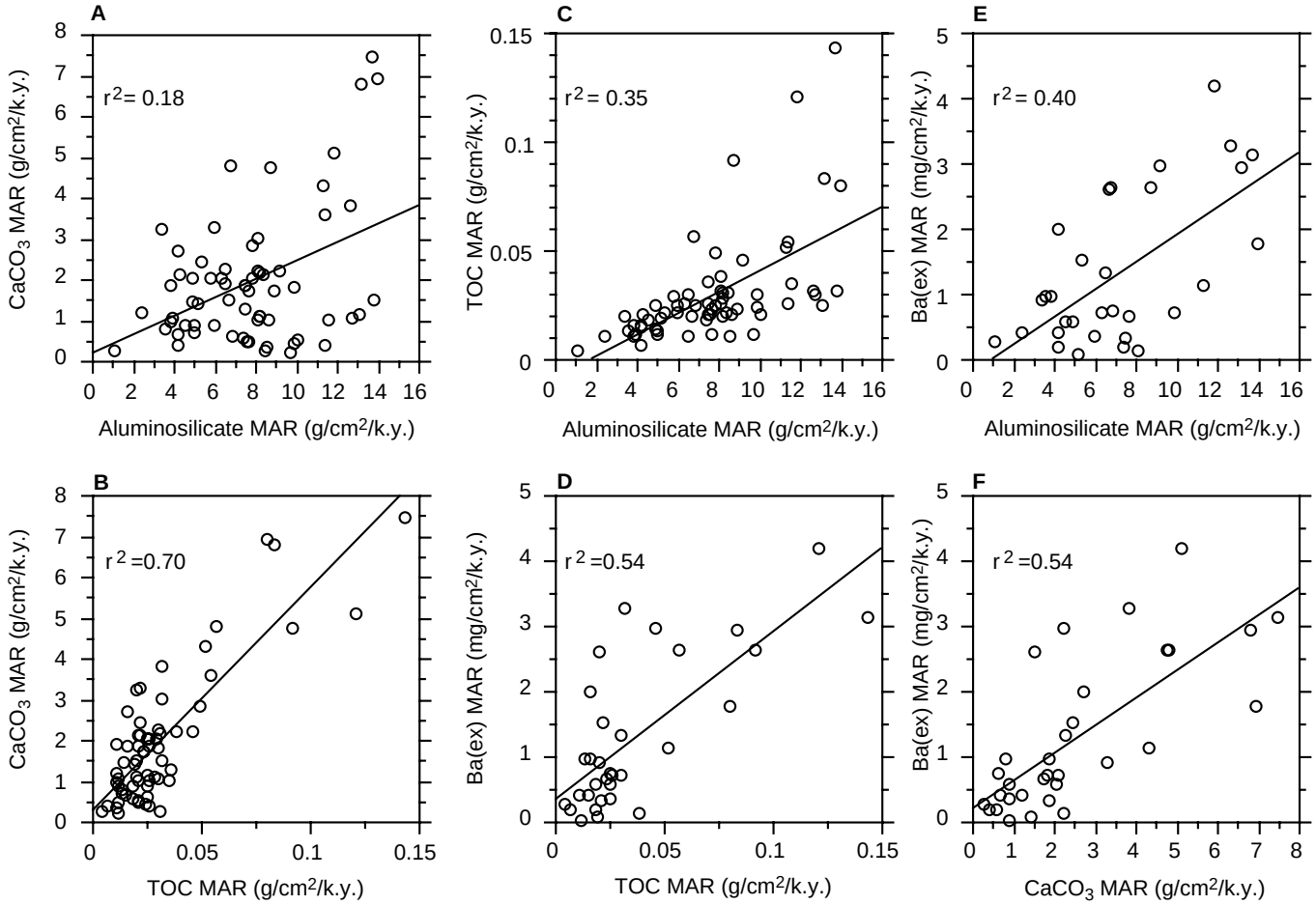

Figure 7. Linear correlation between **(A)** aluminosilicate MAR and $CaCO_3$ MAR, **(B)** TOC MAR and $CaCO_3$ MAR, **(C)** aluminosilicate MAR and TOC MAR, **(D)** TOC MAR and Ba(ex) MAR, **(E)** aluminosilicate MAR and Ba(ex) MAR, and **(F)** $CaCO_3$ MAR and Ba(ex) MAR for Site 983. Correlation estimates for Ba(ex) MAR vs. other components exclude samples where the normative estimation approach failed.

periods. These variations in sediment terrigenous component made estimation of Ba(ex) in some sediment samples difficult.

The correlation between the TOC MAR, $CaCO_3$ MAR, and Ba(ex) MAR—especially in sediments younger than ~600 ka—was stronger than the correlation of any of these components to aluminosilicate MARs. Weak positive correlations between the biogenic components and aluminosilicate MAR could indicate enhanced preservation during times of high total MAR. Given the shallow depth of Site 983 and inferences from published foraminiferal carbon isotopes as a tracer of regional bottom-water masses, large changes in dissolution at this site seem unlikely. These observations suggest that the most plausible causes for the low-frequency carbonate variations observed in the Site 983 sediments are shifts in surface productivity and, to a lesser extent, control by the input of terrigenous material. Deeper in the section (~600–1200 ka), the correlation between Ba(ex) and the other biogenic tracers is weak. This lack of correlation between Ba(ex) and biogenic carbonate likely results from either the higher supply of terrigenous material in older sediments or remobilization of Ba because of very low pore-water sulfate ion concentrations.

ACKNOWLEDGMENTS

Discussions with J. McManus and D. Hodell, who kindly provided their age model for Site 983, and with the shipboard sedimentologists on Leg 162 helped us prepare this chapter. Dr. T. Ishii and Dr. S. Saito of the Ocean Research Institute, University of Tokyo, are thanked for XRF analysis and for their valuable suggestions. We also thank C. Langmuir for providing unpublished geochemical data for Icelandic basalt and for helpful discussions with JDO.

REFERENCES

Bishop, J.K.B., 1988. The barite-opal organic carbon association in oceanic particulate matter. *Nature*, 332:341–343.

Bout-Roumazeilles, V., Debrabant, P., Labeyrie, L., Chamley, H., and Cortijo, E., 1997. Latitudinal control of astronomical forcing parameters on the high-resolution clay mineral distribution in the 45°–60°N range in the North Atlantic Ocean during the past 300,000 years. *Paleoceanography*, 12:671-686.

Channell, J.E.T., Hodell, D.A., McManus, J., and Lehman, B., 1998. Orbital modulation of the Earth's magnetic field intensity. *Nature*, 394:464–468.

Dehairs, F., Chesselet, R., and Jedwab, J., 1980. Discrete suspended particles of barite and the barium cycle in the open ocean. *Earth Planet. Sci. Lett.*, 49:528–550.

Dehairs, F., Goeyns, L., Steoobants, N., Bernard, P., Goyet, C., Poisson, A., and Chesselet, R., 1990. On suspended barite and the oxygen minimum in the Southern Ocean. *Global Biogeochem. Cycles*, 4:85–102.

Dymond, J., 1981. Geochemistry of Nazca Plate surface sediments: an evaluation of hydrothermal, biogenic, detrital, and hydrogenous sources. *In* Kulm, L.D., Dymond, J., Dasch, E.J., Hussong, D.M., and Roderick, R. (Eds.), *Nazca Plate: Crustal Formation and Andean Convergence.* Mem.—Geol. Soc. Am., 154:133–173.

Dymond, J., Suess, E., and Lyle, M., 1992. Barium in deep-sea sediment: a geochemical proxy for paleoproductivity. *Paleoceanography*, 7:163–181.

François, R., Honjo, S., Manganini, S.J., and Ravizza, G.E., 1995. Biogenic barium fluxes to the deep sea: implications for paleoproductivity reconstruction. *Global Biogeochem. Cycles*, 9:289–303.

Frolich, P.N., Klinkhammer, G.P., Bender, M.L., Luedtke, N.A., Heath, G.R., Cullen, D., Dauphin, P., Hartman, B., and Maynard, V., 1979. Early oxidation of organic matter in pelagic sediments of the eastern equatorial Atlantic: suboxic diagenesis. *Geochem. Cosmochem. Acta*, 43:1057–1090.

Gingele, F., and Dahmke, A., 1994. Discrete barium particle and barium as tracers of paleoproductivity in South Atlantic sediments. *Paleoceanography*, 9:151–168.

Gislason, S.R., Arnorsson, S., and Armannsson, H., 1996. Chemical weathering of basalt in southwest Iceland: effects of runoff, age of rocks and vegetative/glacial cover. *Am. J. Sci.*, 296:837–907.

Grousset, F., Latouche, C., and Parra, M., 1982. Late Quaternary sedimentation between the Gibbs fracture and the basin: mineralogical and geochemical data. *Mar. Geol.*, 47:303–330.

Harris, S.E., Mix, A.C., and King, T., 1997. Biogenic and terrigenous sedimentation at Ceara Rise, western tropical Atlantic, supports Pliocene–Pleistocene deep-water linkage between hemispheres. *In* Shackleton, N.J., Curry, W.B., Richter, C., Bralower, T.J. (Eds.), *Proc. ODP, Sci. Reports*, 154: College Station, TX (Ocean Drilling Program), 331–345.

Hyun, S., 1997. Geochemical study for paleoproductivity reconstruction in Northwest Pacific and North Atlantic Ocean [Ph.D. thesis]. Univ. Tokyo.

Jansen, E., Raymo, M.E., Blum, P., et al., 1996. *Proc. ODP, Init. Repts.*, 162: College Station, TX (Ocean Drilling Program).

Lea, D., and Boyle, E.A., 1989. Barium content of benthic foraminifera controlled by bottom-water composition. *Nature*, 338:751–753.

Martin, J., and Knauer, G.A., 1973. The chemical composition of plankton. *Geochim. Cosmochim. Acta*, 37:1639–1653.

Mix, A.C., Rugh, W., Pisias, N.G., Veirs, S., Leg 138 Shipboard Sedimentologists (Hagelberg, T., Hovan, S., Kemp, A., Leinen, M., Levitan, M., Ravelo, C.), and Leg 138 Scientific Party, 1992. Color reflectance spectroscopy: a tool for rapid characterization of deep-sea sediments. *In* Mayer, L., Pisias, N., Janecek, T., et al., *Proc. ODP, Init. Repts.*, 138 (Pt. 1): College Station, TX (Ocean Drilling Program), 67–77.

Müller, P.J., and Suess, E., 1979. Productivity, sedimentation rate, and sedimentary organic matter in the oceans, I. Organic carbon preservation. *Deep-Sea Res. Part A*, 26:1347–1362.

Nagano, S., and Nakashima, S., 1992. The factor controlling vertical color variation of North Atlantic Madeira Abyssal Plain sediment. *Mar. Geol.*, 109:83–94.

Oppo, D.W., and Lehman, S.J., 1993. Mid-depth circulation of the subpolar North Atlantic during the last glacial maximum. *Science*, 259:1148–1152.

Parra, M., Puechmaille, C., Dumon, J.C., Delmont, P., and Ferragne, A., 1986. Geochemistry of Tertiary alterite clay phases on the Iceland-Faeroe Ridge (Northeast Atlantic), Leg 38, Site 336. *Chem.Geol.*, 54:165–176.

Raymo, M., Ganley, K., Carter, S., Oppo, D.W., and McManus, J., 1998. Millenial-scale climate instability during the early Pleistocene epoch. *Nature*, 392:699–702.

Raymo, M., Oppo, D.W., and Curry, W., 1997. The mid-Pleistocene climate transition: a deep sea carbon isotopic perspective. *Paleoceanography*, 12:546–559.

Riley, J.P., and Roth, I., 1971. The distribution of trace elements in some species of phytoplankton grown in culture. *J. Mar. Biol. Assoc. U.K.*, 51:63–72.

Ruddiman, W.F., Bowles, F.A., 1976. Early interglacial bottom-current sedimentation on the eastern Reykjanes Ridge. *Mar. Geol.*, 21:191–210.

Schmitz, B., 1987. Barium, equatorial high productivity, and the northward wandering of the Indian continent. *Paleoceanography*, 2:63–77.

Stein, R., 1990. Organic carbon/sedimentation rate relationship and its paleoenvironmental significance for marine sediments. *Geo-Mar. Lett.*, 10:37–44.

Taylor, S.R., 1964. Abundance of chemical elements in the continental crust: a new table. *Geochem. Cosmochem. Acta*, 28:1273–1285.

Taylor, S.R., and McLennan, S.M., 1985. *The Continental Crust: Its Composition and Evolution:* Oxford (Blackwell Scientific).

Torres, M.E., Brumsack, H.-J., Bohrmann, G., and Emeis, K.C., 1996. Barite fronts in continental margin sediments: a new look at barium remobilization in the zone of sulfate reduction and formation of heavy barites in diagenetic fronts. *Chem. Geol.*, 127:125–139.

von Breymann, M.T., Emeis, K.-C., and Camerlenghi, A., 1990. Geochemistry of sediments from the Peru upwelling area: results from Sites 680, 682, 685, and 688. *In* Suess, E., von Huene, R., et al., *Proc. ODP, Sci. Results*, 112: College Station, TX (Ocean Drilling Program), 491–503.

von Breymann, M.T., Emeis, K.C. and Suess, E., 1992. Water depth and diagenetic constraints on the use of barium as a paleoproductivity indicator. *In* Summerhayes, C.P., Prell, W.L., and Emeis, K.C. (Eds.), *Upwelling Systems: Evolution Since the Early Miocene*. Geol. Soc. Spec. Publ. London, 64:273–384.

Waagstein, R., 1988. Structure, composition and age of the Faeroe basalt plateau. *In* Morton, A.C., and Parson, L.M. (Eds.), *Early Tertiary Volcanism and the Opening of the Northeast Atlantic*. Geol. Soc. Spec. Publ. London, 39:225–238.

Date of initial receipt: 14 August 1997
Date of acceptance: 11 June 1998
Ms 162SR-019